Temperature dependence of magnetic properties of $La_{0.7}Sr_{0.3}MnO_3/SrTiO_3$ thin films on silicon substrates

M. Belmeguenai,[1] S. Mercone,[1] C. Adamo,[2] L. Méchin,[3] C. Fur,[3] P. Monod,[4] P. Moch,[1] and D. G. Schlom[2]
[1]*LPMTM (UPR 9001) CNRS, Université Paris 13, Avenue Jean-Baptiste Clément, 93430 Villetaneuse, France*
[2]*Department of Materials Science and Engineering, Cornell University, Ithaca, New York 14853-1501, USA*
[3]*GREYC (UMR 6072) CNRS, ENSICAEN, Université de Caen Basse-Normandie, 6 Boulevard Maréchal Juin, 14050 Caen Cedex, France*
[4]*LPEM (UPR A0005), ESPCI, 10 Rue Vauquelin, F-75231 Paris Cedex 5, France*
(Received 14 October 2009; revised manuscript received 16 December 2009; published 8 February 2010)

20-nm-thick and 50-nm-thick $La_{0.7}Sr_{0.3}MnO_3$ films were grown by molecular-beam epitaxy on Si (001) substrates overlaid by a 20-nm-thick $SrTiO_3$ (001) buffer layer. X-ray diffraction and atomic force microscopy studies demonstrate their epitaxial (001) orientation. Their static magnetic properties are investigated as a function of the temperature using a superconducting quantum interference device. Ferromagnetic resonance (FMR) inside a cavity and microstrip ferromagnetic resonance (MS-FMR) are used to study their dynamic properties. The field dependence of the MS-FMR resonance frequency as a function of a perpendicular applied field provides a precise evaluation of the g factor and of the effective demagnetizing field $4\pi M_{eff}$ at room temperature. The perpendicular uniaxial and the in-plane anisotropies strongly decrease versus temperature. The excellent epitaxial crystallographic orientation due to the $SrTiO_3$ buffer gives rise to an observed fourfold symmetry of the in-plane anisotropy which is assumed of magnetocrystalline nature. The large perpendicular uniaxial anisotropy gives rise to an effective demagnetizing field significantly larger than the resulting one from the sole contribution of the saturation magnetization. It is most probably induced by the interfacial strain.

DOI: 10.1103/PhysRevB.81.054410 PACS number(s): 75.40.Gb, 76.50.+g, 75.30.Gw, 75.40.Cx

I. INTRODUCTION

Perovskite manganites $[(RE)_{1-x}(AE)_xMnO_3$, where RE =rare earth and AE=alkaline earth] form an interesting class of compounds where the interplay between metal-insulator and ferromagnetic transitions results in a variety of fascinating properties such as colossal magnetoresistance.[1] The origin of ferromagnetism in these materials is the double-exchange interaction[2] which leads to a strong correlation between magnetization and charge transport properties. $La_{0.7}Sr_{0.3}MnO_3$ (LSMO) is one of the perovskite manganites which show a colossal magnetoresistance and is expected to have a spin polarization close to 100% (half metal)[3] allowing for potential technological applications in spin-sensitive devices.

Integrating $La_{0.7}Sr_{0.3}MnO_3$ onto semiconducting materials is a challenging task for potential applications that utilize both information processing and data storage in the same device, such as high-density magnetic memories, sensors, and infrared bolometers. In order to grow an epitaxial quality manganite film on a semiconductor substrate, the film-substrate lattice mismatch needs to be minimized and chemical reactions between the substrate and the deposited film should be eliminated. Recent progress on direct integration[4,5] of $SrTiO_3$ (STO) on Si has opened the possibility of integrating both STO and $La_{0.7}Sr_{0.3}MnO_3$ onto this technologically important semiconductor. Pradhan *et al.*[6] have succeeded in the fabrication of high-performance $La_{0.67}Ba_{0.33}MnO_3$ samples which are ferromagnetic in the vicinity of room temperature. Despite the intense research activity on $La_{0.7}Sr_{0.3}MnO_3$ thin films grown on Si substrates,[7–9] mainly focused on their structural and static magnetic properties, their dynamic magnetic properties remain unexplored, according to our knowledge. The dynamics of these types of materials within the 1–10 GHz frequency range, which determines the high-speed response, is key for their future technological applications, especially in view of increasing data rates in magnetic storage devices. Therefore, the aim of this paper is to investigate the dynamic magnetic properties of $La_{0.7}Sr_{0.3}MnO_3$ thin films deposited on a Si substrate first overlaid with a thin STO buffer.

In this paper, we present static magnetometric measurements, conventional ferromagnetic resonance (FMR) and, in addition, microstrip line ferromagnetic resonance (MS-FMR), thus allowing for a full magnetic characterization of $La_{0.7}Sr_{0.3}MnO_3$ thin films at different temperatures. In the first part of this work, we describe the samples and the experimental setups (Sec. II). In Sec. III, we define the model to be used for the analysis of our measurements. The first part of Sec. IV summarizes the main static magnetic characteristics derived from superconducting quantum interference device (SQUID) data; its second part presents dynamic measurements obtained using FMR and MS-FMR and provides the derived magnetic parameters which satisfactory fit our data. In Sec. V, conclusions are presented.

II. SAMPLES AND EXPERIMENTAL SETUPS

A. Samples

$La_{0.7}Sr_{0.3}MnO_3$ films with 20 and 50 nm thickness were grown on STO buffered Si (001) substrates[5] by a reactive molecular-beam epitaxy system. A substrate temperature of T=670 °C and an ozone background pressure of 3×10^{-7} Torr were used. The x-ray diffraction study shows that both the $La_{0.7}Sr_{0.3}MnO_3$ and STO layers are fully (001) oriented and of high epitaxial quality. θ-2θ scans reveal that no second phases are present. The full width at half maxi-

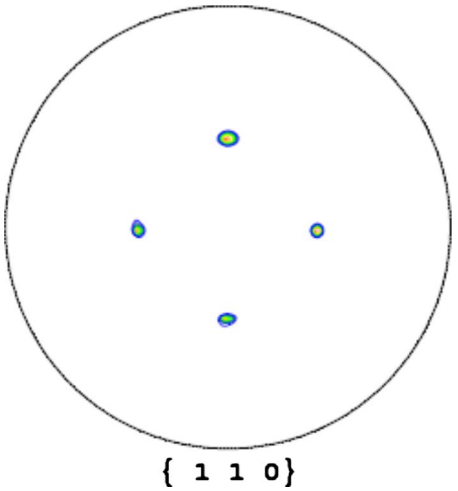

FIG. 1. (Color online) 110 pole figure for the $La_{0.7}Sr_{0.3}MnO_3$ (50 nm)/$SrTiO_3$ (20 nm)/Si film. Directions x and y correspond to [100] and [010], respectively.

mum in ω-scan of the 002 STO and the 002 $La_{0.7}Sr_{0.3}MnO_3$ peaks are 0.26° and 0.22°, respectively. The pole figure of $La_{0.7}Sr_{0.3}MnO_3$ measured around its 110 peak (Fig. 1) shows full in-plane epitaxy of the $La_{0.7}Sr_{0.3}MnO_3$ film with pseudocubic axes [100] and [010] along the sample edges (which define the x axis and the y axis, respectively). Therefore, from the x-ray study, fourfold in-plane anisotropy is expected with one principal axis which can be chosen parallel to [110]. Detailed study of structural properties of these samples will be reported in a forthcoming paper.

B. Experimental setups

The static measurements were carried out using a SQUID sweeping the (4–400 K) temperature range with a maximum applied field of 5 T. The saturation magnetization M_s as a function of temperature was measured. Some conclusions about the anisotropy properties were also obtained from these data.

For the dynamic measurements, 9.5 GHz conventional FMR (Ref. 10) and MS-FMR (Ref. 11) were used. The conventional FMR setup in a bipolar X-band Bruker ESR spectrometer with a TE_{102} resonant cavity immersed is an Oxford cryostat allowing for exploring the 4–300 K temperature interval. The MS-FMR setup consists of a homemade mounting which, up to now, only works at room temperature. The resonance fields (conventional FMR) and frequencies (MS-FMR) are obtained from a fit assuming a Lorentzian derivative shape of the recorded data. In contrast with the conventional FMR, the MS-FMR allows for dynamic measurements over a large frequency range and for the application of low external fields, in order to put in evidence small magnetic anisotropies which cannot be detected using the necessarily high applied magnetic fields used in conventional FMR.

III. MAGNETIC ENERGY-DENSITY MODEL AND EXPRESSIONS FOR THE UNIFORM MAGNETIC MODE

Figure 2 reports the coordinate system used as reference, where φ_M (respectively, φ_H) is the in-plane angle between the magnetization $\boldsymbol{M}$ (respectively, the external applied field $\boldsymbol{H}$) and the x axis while θ_M (respectively, θ_H) is the out-of-plane angle between the magnetization (respectively, the external field $\boldsymbol{H}$) and the direction normal to the sample plane (z axis). We assume fourfold in-plane anisotropy, as expected from the crystallographic orientation (see Sec. II) and we then define φ_4 as the angle between one of the anisotropy axes and the x axis.

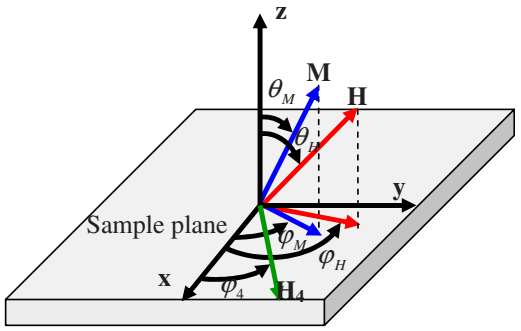

FIG. 2. (Color online) Sketch of the coordinate system used. φ_M (respectively, φ_H) is the in-plane angle between the magnetization $\boldsymbol{M}$ (respectively, the external field $\boldsymbol{H}$) and the x axis while θ_M (respectively, θ_H) is the out-of-plane angle between the magnetization (respectively, the external field H) and the z axis and φ_4 is the angle of fourfold in-plane anisotropy axis H_4 with the x axis. $H_4=\frac{4K_4}{M_s}$ is the fourfold in-plane anisotropy field.

The free-energy density E is then written as

$$E = -M_s H[\sin\theta_M \sin\theta_H \cos(\varphi_M - \varphi_H) + \cos\theta_M \cos\theta_H] - (2\pi M_s^2 - K_\perp)\sin^2\theta_M - \frac{1}{8}K_4[3 + \cos 4(\varphi_M - \varphi_4)]\sin^4\theta_M. \quad (1)$$

M_s is the magnetization at saturation. $K_\perp$ and K_4 are the uniaxial out-of-plane and the in-plane anisotropy constant, respectively. $K_\perp$ and K_4 are effective anisotropy constants resulting from the simultaneous occurrence of a true volume term and of the additional contribution of a surface energy term. More explicitly, $K_\perp = K_{\perp V} + (K_{\perp S})/d$ and $K_4 = K_{4V} + (K_{4S})/d$, where d is the film thickness and where the indices V and S are related to the volume and to the surface contribution, respectively. It is easily proved that, in the case of small thickness values, as considered in this study, this approach using effective volume energy density allows for a satisfactory evaluation of the frequencies of the magnetic modes.[12]

The resonance frequency F_r of the uniform precession mode is deduced from the energy density from the expression[13]

$$F_r^2 = \left(\frac{\gamma}{2\pi}\right)^2 \frac{1}{M_s^2 \sin^2\theta_M}\left[\frac{\partial^2 E}{\partial\theta_M^2}\frac{\partial^2 E}{\partial\varphi_M^2} - \left(\frac{\partial^2 E}{\partial\theta_M\,\partial\varphi_M}\right)^2\right], \quad (2)$$

where γ is the gyromagnetic factor ($\gamma = g\,\mu_B$, μ_B being the Bohr magneton and g being the Landé factor) and where the derivatives are evaluated at the equilibrium position.

In the case of an in-plane applied magnetic field, the magnetization lies in the plane of the film, $\theta_M=\theta_H=90°$. The in-plane resonance frequency is then given by

$$F_r^2=\left(\frac{\gamma}{2\pi}\right)^2\left[H\cos(\varphi_M-\varphi_H)+4\pi M_{eff}+\frac{K_4}{2M_S}(3+\cos 4(\varphi_M-\varphi_4))\right]\times\left[H\cos(\varphi_M-\varphi_H)+\frac{2K_4}{M_S}\cos 4(\varphi_M-\varphi_4)\right], \quad (3)$$

where $4\pi M_{eff}=4\pi M_s-\frac{2K_\perp}{M_s}$ defines the effective demagnetizing field.

The φ_M value is calculated from the energy minimization at equilibrium. It is a solution of

$$H\sin(\varphi_{\mathrm{M}}-\varphi_{\mathrm{H}})=\frac{1}{2}\frac{K_4}{M_s}\sin 4\varphi_{\mathrm{M}}. \quad (4)$$

In the case of an out-of-plane applied magnetic field, for θ_H significantly smaller than 90°, high applied fields are needed and, consequently, the fourfold anisotropy contribution can be neglected. It results that the resonance frequency for an out-of-plane applied magnetic field is given by

$$F_{out}^2=\left(\frac{\gamma}{2\pi}\right)^2[H\cos(\theta_M-\theta_H)-4\pi M_{eff}\cos 2\theta_M]\times[H\cos(\theta_M-\theta_H)-4\pi M_{eff}\cos^2\theta_M] \quad (5)$$

with

$$H\sin(\theta_M-\theta_H)=2\pi M_{eff}\sin 4\theta_M. \quad (6)$$

IV. RESULTS AND DISCUSSION

A. Static magnetic properties

The saturation magnetizations of the 20 nm and the 50 nm samples were measured using the SQUID up to 400 K. The values obtained for $4\pi M_s$, under an in-plane applied field of 5000 Oe, at room temperature are 3000 and 2500 Oe, respectively, for the 20-nm-thick and for the 50-nm-thick films, with an error bar which can reach 10%, mostly due to the limited precision concerning the evaluation of the corrections arising from the poorly controllable contribution of the substrate. Typical temperature dependences of $4\pi M_s$ are shown in Fig. 3(a) for the 20-nm-thick and 50-nm-thick films. The measured Curie temperature T_c is the same, 330 K, for both films. A theoretical estimation of the low-temperature magnetization at saturation M_{s0} leads to $4\pi M_{s0}=7350$ Oe (assuming a mean kinetic momentum equal to 11/6 and a Landé factor equal to 2). Within the frame of the experimental precision this value fits our measurement for the 50-nm-thick sample (7900 Oe) but is slightly larger in the case of the 20-nm-thick film (6100 Oe). Such a reduction in the magnetization in thin films is frequently observed.[9,14] Both samples (20 and 50 nm) show a saturation magnetization nearer from the theoretically expected one and significantly higher than the previously reported values in comparable situations (e.g., $La_{0.7}Sr_{0.3}MnO_3$ films grown on a $LaAlO_3$ substrate[14]). As shown in Fig. 3(a), a classical fit of the temperature dependence of $M_s(T,H)$ using a Brillouin function B_J (with $J=1.5$ or 2) provides a reasonable agreement with the experimental data assuming $T_c=330$ K. In the case of the 50-nm-thick film, the best fit is obtained using the above-mentioned 7350 Oe theoretical value of $4\pi M_{s0}$; however, a reduced value of $4\pi M_{s0}$ (5900 Oe) has to be used for the 20-nm-thick sample.

The room-temperature hysteresis loop using an in-plane applied magnetic field along the sample diagonal ([110] direction) shows a rectangular shape with a coercive field of about 7 Oe, as illustrated in Fig. 3(b) for the 50-nm-thick sample. This suggests a weak planar anisotropy but the static data do not allow a convincing quantitative determination of in-plane anisotropy parameters which monitor the magnetic energy density. Moreover, hysteresis loops obtained using a magnetic field parallel to the [100] and to the [010] axes do not appreciably differ from each other. These loops do not behave in the same way as the observed one applying a magnetic field along the [110] axis; their shape is smoother and the measured coercive field is smaller. This result qualitatively agrees with a description of the in-plane anisotropy in terms of a fourfold contribution with an easy axis along the [110] direction (and, indeed, a hard axis along the [100] one).

When the applied field is normal to the film, the magnetization loops roughly agree with the usual scheme of a coherent rotation in the hard-axis geometry, as shown in Fig. 3(c). The effective demagnetizing field $H_{eff}=4\pi M_{eff}$ is found to lay around 5000 Oe for the 50-nm-thick film. However, it cannot be derived precisely.

B. Dynamic magnetic properties

In principle, both FMR and MS-FMR can give access to all the coefficients which define the magnetic energy density. However, the g value, which determines the gyromagnetic factor γ, is precisely accessible only by the MS-FMR technique, through the study of the frequency variation versus the amplitude of an applied magnetic field perpendicular to the film. More generally, MS-FMR provides more accurate evaluations of the magnetic parameters since it allows for experimental studies not only versus the direction of the applied field, as in the case of conventional FMR, but also versus its amplitude. The magnetic parameters where precisely derived at room temperature from MS-FMR measurements. Their variation versus temperature was studied using conventional FMR, except in the case of the g factor which could not be precisely evaluated through this technique. Fortunately, g is expected to be practically independent of the temperature,[15] as assumed in the present work.

1. Room-temperature (300 K) results

For both films (20 and 50 nm) we find $g=1.915$. This value is slightly smaller than the theoretically expected one (≈ 2) which is generally observed in bulk $La_{0.7}Sr_{0.3}MnO_3$.[15] Both films approximately show the same effective demagnetizing field.

For the 50 nm film the best fit obtained from the MS-FMR study under a perpendicular magnetic field corresponds

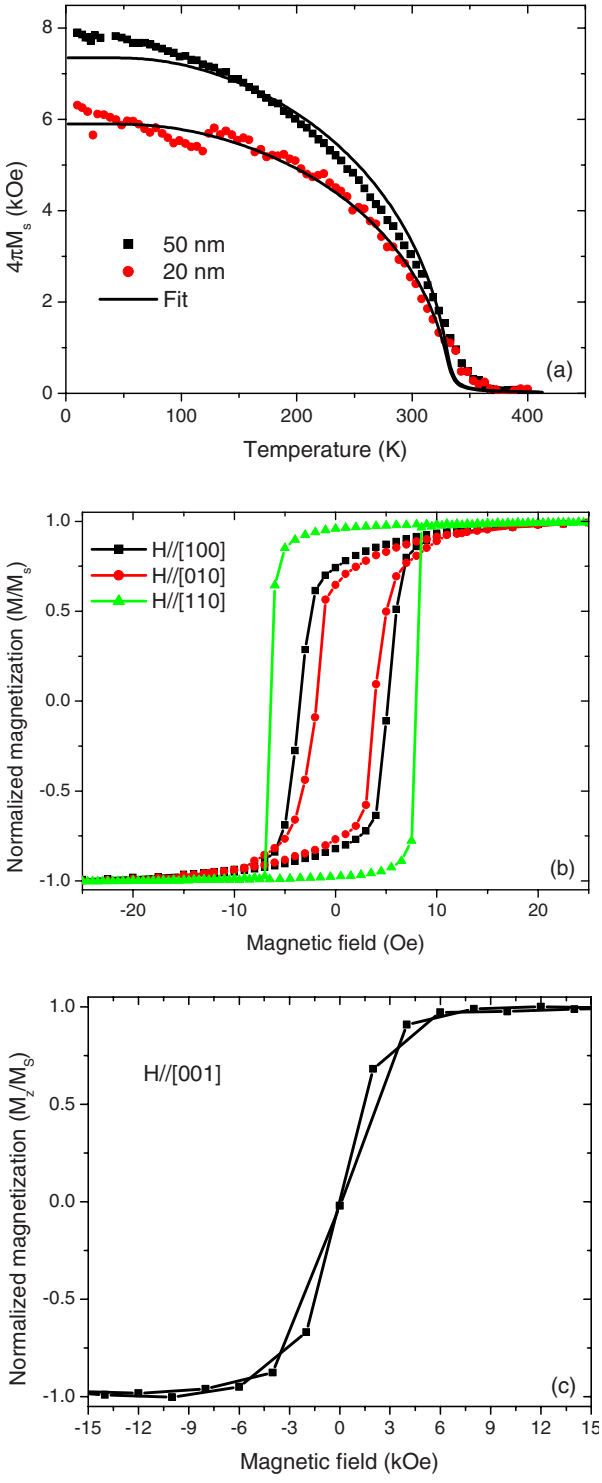

FIG. 3. (Color online) (a) Temperature dependences of $4\pi M_s$ in a $La_{0.7}Sr_{0.3}MnO_3$ (50 nm)/$SrTiO_3$ (20 nm)/Si sample and a $La_{0.7}Sr_{0.3}MnO_3$ (20 nm)/$SrTiO_3$ (20 nm)/Si film measured under a 5000 Oe in-plane applied field; the full black lines represent the best obtained fit using a simple molecular-field model (see text). (b) Room-temperature hysteresis loops for three different orientations of an in-plane applied magnetic field in the $La_{0.7}Sr_{0.3}MnO_3$ (50 nm)/$SrTiO_3$ (20 nm)/Si sample. (c) Room-temperature hysteresis loops for an applied magnetic field perpendicular to the $La_{0.7}Sr_{0.3}MnO_3$ (50 nm)/$SrTiO_3$ (20 nm)/Si sample plane.

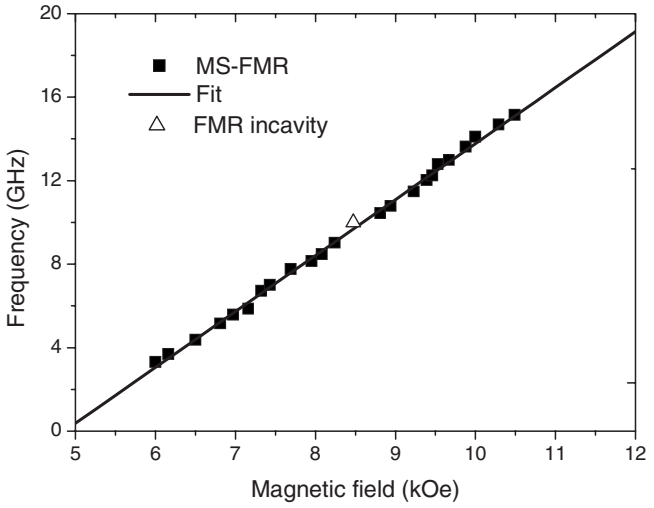

FIG. 4. MS-FMR resonance frequency dependence on the amplitude of a perpendicular applied magnetic field in the $La_{0.7}Sr_{0.3}MnO_3$ (50 nm)/$SrTiO_3$ (20 nm)/Si sample.

to $4\pi M_{eff}$=4900 Oe. Taking account of the static magnetization reported above it results that $K_\perp$ is negative (thus implying an easy-axis uniaxial anisotropy with an anisotropy field $H_\perp = \left|2\frac{K_\perp}{M_s}\right|$ of about 2000 Oe)

From the MS-FMR measurements of the frequency dependence versus the direction of an in-plane applied field we deduce that φ_4=45°, as expected, and that this angle is related to the easy in-plane anisotropy axis. For the 50-nm-thick sample the corresponding measured anisotropy field $H_4 = 4\frac{K_4}{M_s}$ is equal to 28 Oe.

Figures 4 and 5 illustrate that the obtained parameters allow for an excellent fit of all the experimental data for fields applied perpendicular (Fig. 4) as well as parallel to the films [Figs. 5(a) and 5(b)], including conventional FMR results.

2. Temperature dependence

The variations in the resonance fields versus their orientation for both samples was studied by conventional FMR as a function of the temperature in view of deriving the temperature dependence of the effective demagnetizing field and of the uniaxial and in-plane anisotropy parameters. Figure 6(a) shows a typical spectrum at 120 K for 50-nm-thick film while Fig. 6(b) presents angular variations in the resonance fields in this sample at the same temperature. Two distinct modes noted 1 and 2 are observed. We begin by focusing on the so-called "principal" mode 1 while mode 2 will be discussed in the end of this section.

The derived values of the effective demagnetizing fields of the 20 nm and of the 50 nm films do not appreciably differ from each other. These values can be obtained from in-plane and, when the resonant field does not overpass the experimentally available maximum value (16000 Oe), from out-of-plane measurements. In the 20-nm-thick and the 50-nm-thick samples, they are decreasing functions of the temperature, varying from about 14000 Oe at 4 K down to 5000 Oe at 300K, as shown in Fig. 7. The evaluation of the perpendicu-

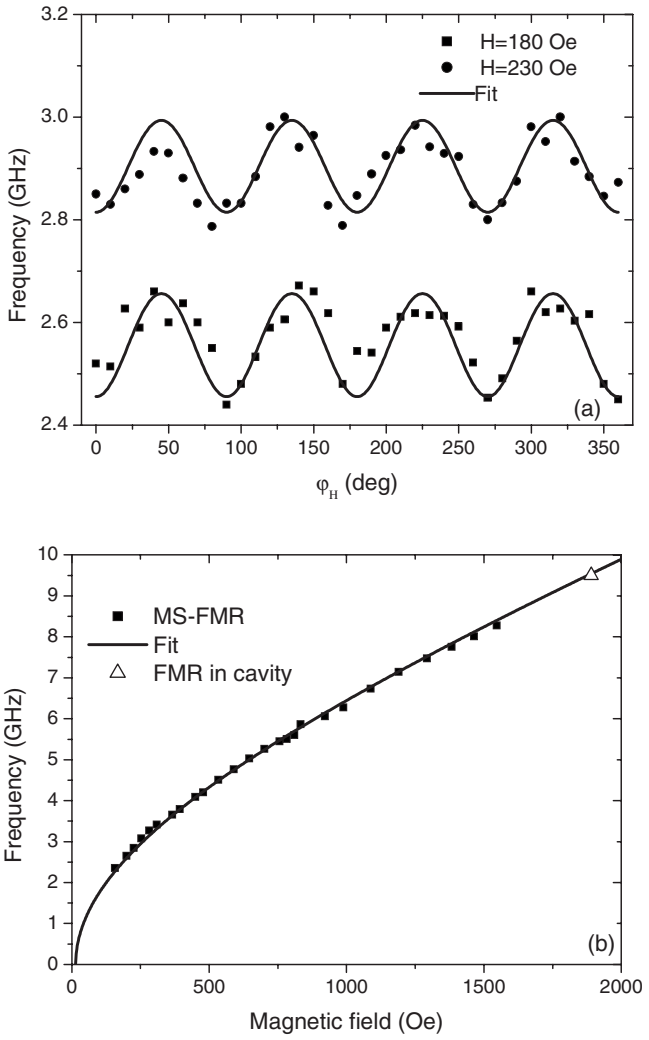

FIG. 5. (a) MS-FMR in-plane angular dependence of the resonance frequency. (b) Resonance frequency of the uniform mode as a function of the in-plane applied field (parallel to the x axis) in the $La_{0.7}Sr_{0.3}MnO_3$ (50 nm)/$SrTiO_3$ (20 nm)/Si sample.

lar uniaxial anisotropy suffers from a rather a low accuracy, due to the lack of precision concerning the evaluation of the magnetization (see the preceding section). However, its approximate variation versus temperature is shown in Fig. 8(a); the perpendicular uniaxial easy-axis anisotropy field $H_\perp$ decreases from about 5000 Oe down to 2000 Oe when T increases from 4 to 300 K. As mentioned above the $K_\perp$ coefficient is negative. Figure 8(b) presents the resulting temperature variation in $|K_\perp|$; in both samples it approximately linearly decreases above 120 K from about 1.5×10^6 erg/cm^3 down to 2.5×10^5 erg/cm^3 at 300 K. Large negative values of $K_\perp$ have been observed previously in $La_{0.7}Sr_{0.3}MnO_3$ films grown on a $SrTiO_3$ substrate.[10] The main source of uniaxial perpendicular anisotropy is generally considered as proceeding from the interfacial strain through the magnetoelastic coupling.[10,14] Notice that its sign depends on the sign of the mismatch between the lattice constants of $La_{0.7}Sr_{0.3}MnO_3$ and the substrate; it was found positive in the case of $LaAlO_3$ (compressive strain)[14] but it is negative in the case of STO (extensive strain).[10]

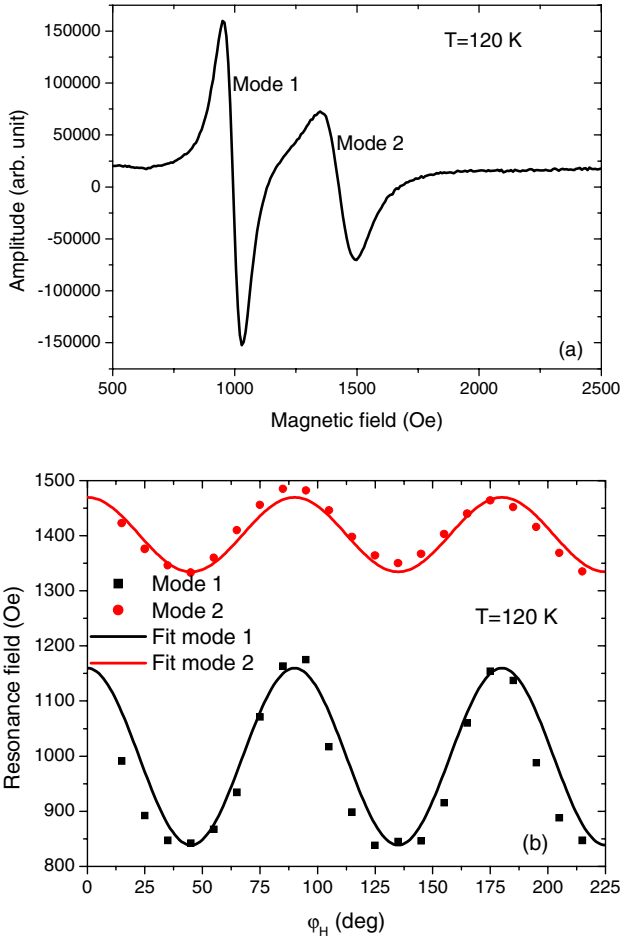

FIG. 6. (Color online) (a) FMR spectrum for an in-plane applied magnetic field (φ_H=15°). (b) In-plane angular dependence of the two observed resonance fields. All the measurements are performed at 120 K on the $La_{0.7}Sr_{0.3}MnO_3$ (50 nm)/$SrTiO_3$ (20 nm)/Si sample. The two distinct fits are obtained using (i) $4\pi M_{eff}$ =11450 Oe, H_4=340 Oe for mode 1 and (ii) $4\pi M_{eff}$=7500 Oe, H_4=150 Oe for mode 2.

The temperature variation in the fourfold in-plane anisotropy field was also studied and it is shown in Fig. 9(a); in both films the easy axis remains along the [110] direction (i.e., φ_4=45° and $H_4 > 0$). Within the experimental accuracy the 20-nm-thick and the 50-nm-thick samples show identical values of the coefficient K_4 in the full studied temperature range, as shown in Fig. 9(b); it decreases from about 1.4×10^5 erg/cm^3 at 4 K down to 10^4 erg/cm^3 at 300 K. This result is in agreement with previously reported observations in $La_{0.7}Sr_{0.3}MnO_3$ thin films on STO (001) substrates[16,17] and with the symmetry put in evidence by our x-ray diffraction spectra and by Kerr microscopy;[18] it suggests that this in-plane anisotropy, induced by the (001) STO seed layer, is of magnetocrystalline nature. The values of K_4 at 100 K reported in Ref. 14 for a large manifold of $La_{0.7}Sr_{0.3}MnO_3$ films deposited on different substrates allowing for a fourfold in-plane symmetry lie in the $[3.9 \times 10^4, 13 \times 10^4]$ erg/cm^3 interval, to compare to our own determination, 8.5×10^4 erg/cm^3. In addition, they report nearly the same decrease versus temperature as the observed one in the present study.

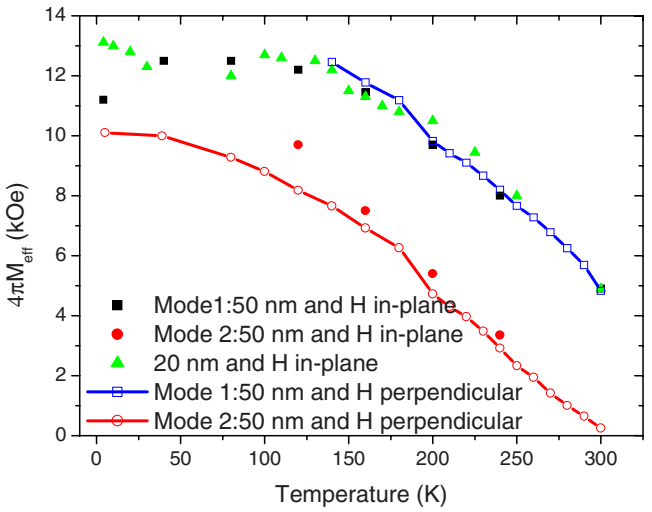

FIG. 7. (Color online) Temperature dependence of the effective demagnetizing field in the $La_{0.7}Sr_{0.3}MnO_3$ (50 nm)/$SrTiO_3$ (20 nm)/Si sample and in the $La_{0.7}Sr_{0.3}MnO_3$ (20 nm)/$SrTiO_3$ (20 nm)/Si sample. The results are obtained from the fit of the experimental data using perpendicular and in-plane applied fields.

Since the measured values of $K_\perp$ and K_4 do not appreciably differ for the two studied samples with different thicknesses, we deduce that the main contribution to the anisotropy derives from the volume terms and that the surface energy plays a minor role. The variations in the normalized anisotropy constants $k_\perp = K_\perp(T)/K_\perp(T_0)$ (with T_0=4 K) and $k_4 = K_4(T)/K_4(T_0)$ versus the normalized saturation magnetization $m = M_s(T)/M_s(T_0)$ are reported in Figs. 10(a) and 10(b); the observed behavior is approximately given by $k_\perp = m^2$ and $k_4 = m^6$, respectively. As usual,[19] the anisotropy coefficients show a relative decrease versus temperature significantly faster than the observed one for the magnetization. This decrease is more pronounced for the fourfold term K_4 than for the uniaxial one $K_\perp$.

For simplicity, in the above discussion we omitted to mention the presence of two distinct resonant fields in the thicker film (50 nm), as illustrated in Fig. 6. This multiplicity is observed in the 140–300 K temperature range when applying a magnetic field perpendicular to the sample, and in the 120–200 K temperature range in the case of an in-plane applied field. In order to interpret the data in this sample we had to identify the principal uniform mode within this multifields temperature interval; it is defined as the mode presenting a continuous variation in the resonance field around the boundaries of this interval. Its resonance field is close to the measured one in the 20-nm-thick film, which argues for the validation of this choice. In the perpendicular geometry the principal uniform mode corresponds to the higher measured field; at low temperature it disappears from the spectra due to the limited available value of the applied field. The failure to observe the secondary resonance outside the 120–200 K temperature range is not yet completely understood. For this extra resonance, the measured field value and its variation versus the angular orientation prevent for its identification in terms of a standing magnetic mode along the direction normal to the sample. We then believe that, in this

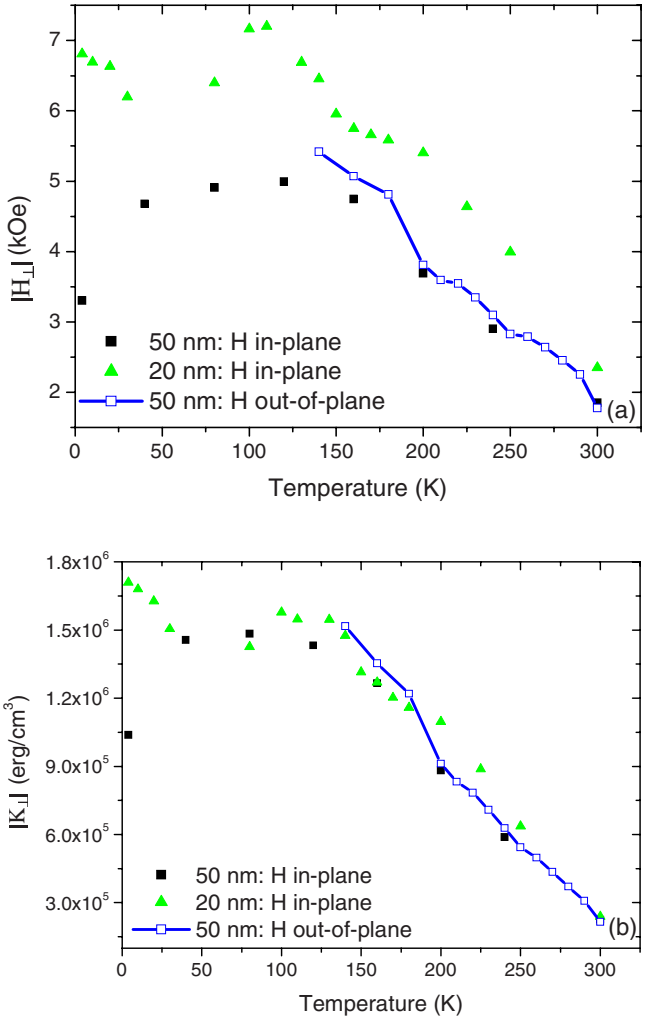

FIG. 8. (Color online) Temperature dependence of the absolute value (a) of the perpendicular uniaxial anisotropy field and (b) of the related anisotropy coefficient $K_\perp$ in the $La_{0.7}Sr_{0.3}MnO_3$ (50 nm)/$SrTiO_3$ (20 nm)/Si sample and in the $La_{0.7}Sr_{0.3}MnO_3$ (20 nm)/$SrTiO_3$ (20 nm)/Si sample. The results are obtained from the fit of the experimental data using perpendicular and in-plane applied magnetic fields.

sample, two different magnetic phases coexist, thus giving rise to two observable uniform modes: the standard principal one (mode 1 in Figs. 6 and 7) which is always present (for an in-plane applied field) and the extra "auxiliary" phase (mode 2) which needs specific thickness conditions in order to be stabilized. The uniform mode related to this auxiliary phase can be studied in order to derive the effective demagnetizing field and the in-plane anisotropy related to this phase as shown in Figs. 7 and 9(a). The effective demagnetizing fields which provide the best fit for the spectra obtained with an in-plane applied magnetic field agree with the derived ones in the case of a perpendicular applied field, as seen in Fig. 7. Also notice that the in-plane anisotropy remains fourfold with an easy axis along [110] but that for the mode 2 the in-plane anisotropy field H_4 is smaller than for the mode 1. It is not possible to evaluate the uniaxial perpendicular anisotropy field $H_\perp$ for this phase since its saturation magnetization cannot be measured separately. Finally, the simultaneous

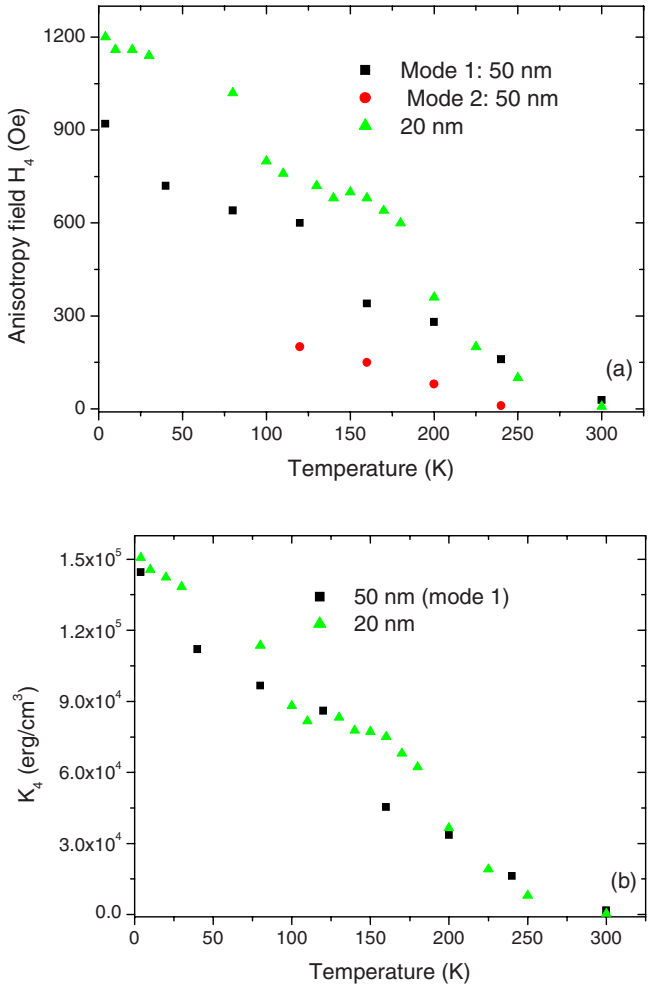

FIG. 9. (Color online) Temperature dependence (a) of the in-plane fourfold anisotropy field and (b) the related anisotropy coefficient K_4 in the $La_{0.7}Sr_{0.3}MnO_3$ (50 nm)/$SrTiO_3$ (20 nm)/Si sample and in the $La_{0.7}Sr_{0.3}MnO_3$ (20 nm)/$SrTiO_3$ (20 nm)/Si sample.

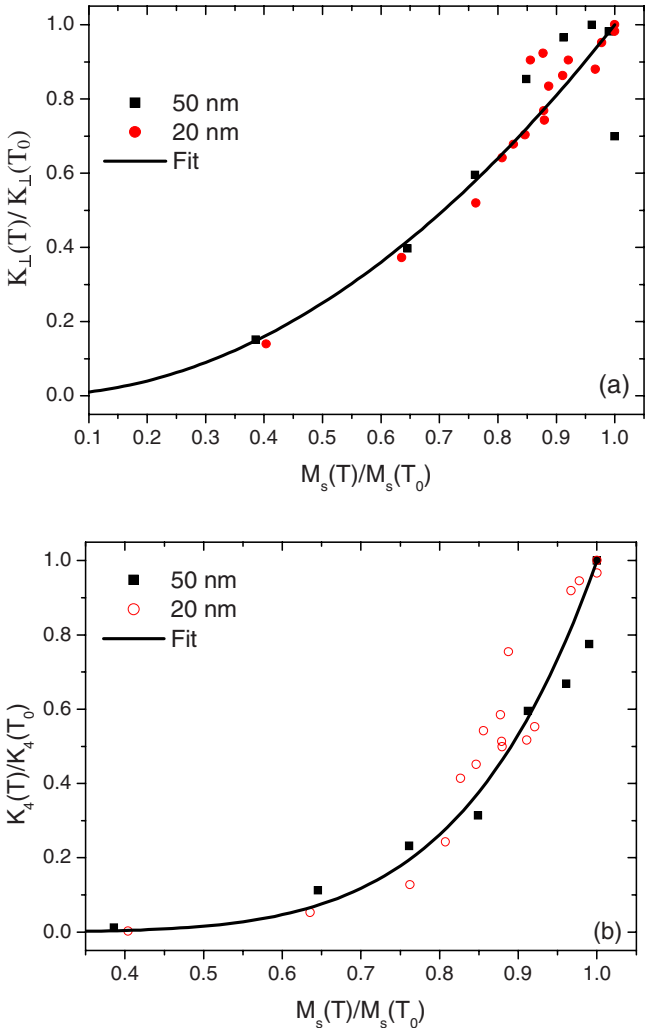

FIG. 10. (Color online) (a) Normalized perpendicular uniaxial anisotropy coefficient $k_\perp = K_\perp(T)/K_\perp(T_0 = 4\ \text{K})$ and (b) normalized in-plane fourfold anisotropy coefficient $k_4 = K_4(T)/K_4(T_0 = 4\ \text{K})$ as a function of the normalized magnetization $m = M_s(T)/M_s(T_0 = 4\ \text{K})$ for the 20-nm-thick and 50-nm-thick samples.

presence of two phases could slightly modify the above determined values of $K_\perp$ and of K_4 related to the principal mode since the SQUID measurements do not allow for separate evaluations of the two involved magnetizations. However, we believe that the apparent adequacy of our classical analysis of the magnetic static measurements argues for the hypothesis of a weak perturbation arising from the auxiliary phase in the calculation of the static magnetic properties of the principal one.

V. CONCLUSION

The temperature dependence of the static and of the dynamic magnetic properties of 20-nm-thick and 50-nm-thick $La_{0.7}Sr_{0.3}MnO_3$ films, deposited on Si substrates overlaid by a 20-nm-thick STO buffer layer have been studied, using SQUID and ferromagnetic resonance (conventional inside cavity: FMR and microstrip line: MS-FMR), respectively. Our x-ray diffraction measurements show an excellent epitaxial (001) orientation of the $La_{0.7}Sr_{0.3}MnO_3$ films. Their magnetic behavior is interpreted assuming a magnetic energy density characterized by a strong uniaxial anisotropy along the direction normal to the plane of the films and by an in-plane anisotropy showing a fourfold symmetry. The in-plane and out-of-plane anisotropies decrease drastically when the temperature increases. A good fit of all the experimental data, using appropriate values of the magnetic coefficients describing the free energy, is obtained. The dependence of the anisotropies on the nature of the buffer layer will be studied in future work.

ACKNOWLEDGMENT

The authors would like to thank T. Chauveau for some x-ray measurements during this study. C.A. and D.G.S. acknowledge the financial support of the National Science Foundation through Grant No. ECCS-0708759.

[1] M. B. Salamon and M. Jaime, Rev. Mod. Phys. **73**, 583 (2001).
[2] C. Zener, Phys. Rev. **82**, 403 (1951).
[3] M. Bowen, M. Bibes, A. Barthélémy, J.-P. Contour, A. Anane, Y. Lemaître, and A. Fert, Appl. Phys. Lett. **82**, 233 (2003).
[4] R. A. McKee, F. J. Walker, and M. F. Chisholm, Phys. Rev. Lett. **81**, 3014 (1998).
[5] Y. Wang, C. Ganpule, B. T. Liu, H. Li, K. Mori, B. Hill, M. Wuttig, R. Ramesh, J. Finder, Z. Yu, R. Droopad, and K. Eisenbeiser, J. Appl. Phys. **93**, 4521 (2003).
[6] A. K. Pradhan, S. Mohanty, Kai Zhang, J. B. Dadson, E. M. Jackson, D. Hunter, R. R. Rakhimov, G. B. Loutts, Jun Zhang, and D. J. Sellmyer, Appl. Phys. Lett. **86**, 012503 (2005).
[7] I. Bergenti, V. Dediu, E. Arisi, M. Cavallini, J. F. Moulin, F. Biscarini, M. De Jong, C. Dennis, and J. Gregg, Prog. Solid State Chem. **33**, 293 (2005).
[8] I. Bergenti, V. Dediu, M. Cavallini, E. Arisi, A. Riminucci, and C. Taliani, Curr. Appl. Phys. **7**, 47 (2007).
[9] A. K. Pradhan, D. Hunter, T. Williams, B. Lasley-Hunter, R. Bah, H. Mustafa, R. Rakhimov, J. Zhang, D. J. Sellmyer, E. E. Carpenter, D. R. Sahu, and J.-L. Huang, J. Appl. Phys. **103**, 023914 (2008).
[10] M. Golosovsky, P. Monod, P. K. Muduli, and R. C. Budhani, Phys. Rev. B **76**, 184413 (2007).
[11] M. Belmeguenai, F. Zighem, Y. Roussigné, S.-M. Chérif, P. Moch, K. Westerholt, G. Woltersdorf, and G. Bayreuther, Phys. Rev. B **79**, 024419 (2009).
[12] Y. Roussigné, F. Ganot, C. Dugautier, P. Moch, and D. Renard, Phys. Rev. B **52**, 350 (1995).
[13] O. Acher, S. Queste, M. Ledieu, K.-U. Barholz, and R. Mattheis, Phys. Rev. B **68**, 184414 (2003).
[14] K. Steenbeck, T. Habisreuther, C. Dubourdieu, and J. P. Sénateur, Appl. Phys. Lett. **80**, 3361 (2002).
[15] V. A. Ivanshin, J. Deisenhofer, H.-A. Krug von Nidda, A. Loidl, A. A. Mukhin, A. M. Balbashov, and M. V. Eremin, Phys. Rev. B **61**, 6213 (2000).
[16] K. Steenbeck and R. Hiergeist, Appl. Phys. Lett. **75**, 1778 (1999).
[17] L. M. Berndt, V. Balbarin, and Y. Suzuki, Appl. Phys. Lett. **77**, 2903 (2000).
[18] P. Lecoeur, P. L. Trouilloud, G. Xiao, A. Gupta, G. Q. Gong, and X. W. Li, J. Appl. Phys. **82**, 3934 (1997).
[19] M. Farle, Rep. Prog. Phys. **61**, 755 (1998).